Journal of Physics and Chemistry of Solids 76 (2015) 45–50

Contents lists available at ScienceDirect

Journal of Physics and Chemistry of Solids

journal homepage: www.elsevier.com/locate/jpcs

Structural, optoelectronic, infrared and Raman spectra from first principles calculations of γ-$Cd(OH)_2$

J.M. Henriques [a], C.A. Barboza [b], E.L. Albuquerque [b], U.L. Fulco [b,*], E. Moreira [c]

[a] Centro de Educação e Saúde, Universidade Federal de Campina Grande, Campus Cuité, 58175-000 Cuité-PB, Brazil
[b] Departamento de Biofísica e Farmacologia, Universidade Federal do Rio Grande do Norte, 59072-970 Natal-RN, Brazil
[c] Universidade Federal Rural do Semi-Árido, Campus Angicos, 59515-000 Angicos-RN, Brazil

ARTICLE INFO

Article history:
Received 11 April 2014
Received in revised form
10 July 2014
Accepted 4 August 2014
Available online 19 August 2014

Keywords:
A. Semiconductor
C. Ab initio calculations
C. Raman spectroscopy
D. Electronic structure
D. Optical properties

ABSTRACT

We have investigated the physical properties of the cadmium hydroxide polymorph γ-$Cd(OH)_2$ using density-functional theory (DFT) considering both the local density and generalized gradient approximations, LDA and GGA, respectively. The electronic band structure, the electronic density of states, the dielectric function and the optical absorption are calculated. A comparison reveals good agreement of the calculated lattice parameters with experimental results. A direct band gap $E(\Gamma \rightarrow \Gamma) = 1.70$ eV (1.53 eV) was obtained within the GGA (LDA) level of calculation. The vibrational normal modes as well as the Raman and infrared spectra of γ-$Cd(OH)_2$ were obtained and assigned.

1. Introduction

Cadmium hydroxide [$Cd(OH)_2$] plays an important role in the functioning of the nickel-cadmium battery, being indeed the anode active ingredient of the accumulator discharged state [1]. It has three different polymorphs, namely the α, β, and γ phases. The polymorph α-$Cd(OH)_2$ hardly crystallizes, whereas the β-$Cd(OH)_2$ one has a hexagonal crystal structure of brucite type. The γ-$Cd(OH)_2$ polymorph, object of this work, has a unique crystal structure, different from the C6 type, as discovered by Glemer et al. [2]; its crystal structure was determined by De Wolf [3].

Several experimental works based on X-ray diffraction (XRD) and Raman spectra measurements ensure that the γ-$Cd(OH)_2$ polymorph is a stable material, with a three-dimensional linkage involving weak hydrogen bonds in a roughly octahedral coordination and sharper diffraction lines [4,5]. Looking for future electronic and optoelectronic technological devices, single-crystalline γ-$Cd(OH)_2$ polymorph nanowires were synthesized at 150 °C by a simple hydrothermal method using aqueous $Cd(NO_3)_2$ as precursor [6]. Furthermore, the use of compounds like NaOH after the hydrolysis of disodium tetrahydroxocadmiate $Na_2Cd(OH)_4$ gives rise to a stable γ-$Cd(OH)_2$ phase, allowing us to consider further theoretical and experimental structural studies of its physical properties [7].

The γ-$Cd(OH)_2$ polymorph is a wide band gap semiconductor with a wide range of possible applications, including solar cells, photo transistors and diodes, transparent electrodes, sensors, cathode electrode materials of batteries, and so forth [8–11]. The applications of γ-$Cd(OH)_2$ are based on its specific optical and electrical properties. For example, $Cd(OH)_2$ films show high electrical conductivity as well as high transparency in the visible region of solar spectrum. Cadmium hydroxide has also been proven to be an important precursor that can be either converted into cadmium oxide through dehydration, or into other functional materials (e.g., CdS, CdSe) by reaction with appropriate elements or compounds [12]. Thin films of γ-$Cd(OH)_2$ have high transparency in the visible region and a high electrical conductivity.

It has also been determined that the cadmium hydroxide can be converted into a cadmium oxide (CdO), which is an important n-type semiconductor with a direct band gap of 2.5 eV and indirect band gap of 1.98 eV [13], by dehydration or by reaction with elements or suitable compounds. It is a promising candidate for optoelectronics applications and can be used in the fabrication of many devices [14–16]. In the past decade, CdO of multifarious 1-D nanostructures (such as nanowires [17], octahedrons and nanowires on micro-octahedrons [18], porous nanobelts [19], nanoneedles [20], and nanostrands [21]) have been synthesized and studied.

Although several works have been reported about the synthesis of γ-$Cd(OH)_2$ in many electronic devices, little is known about their vibrational, optical, electronic and thermal properties. To fill this gap, it is the aim of this work to investigate the physical

* Corresponding author. Tel.: +55 84 3215 3419.
E-mail address: umbertofulco@gmail.com (U.L. Fulco).

http://dx.doi.org/10.1016/j.jpcs.2014.08.003
0022-3697/

properties of the cadmium hydroxide polymorph γ-$Cd(OH)_2$ using quantum chemistry approach (density functional theory-DFT) considering both the local density and generalized gradient approximations, LDA and GGA, respectively. The electronic band structure, the electronic density of states, the dielectric function and the optical absorption are calculated. A comparison with experimental data reveals good agreement with our computational predictions.

The plan of this paper is as follows: in Section 2 we present our computer calculation methodology. Section 3 deals with the main results regarding the physical properties of γ-$Cd(OH)_2$ polymorph, including its geometry optimization, a detailed calculation of its electronic band structure and density of states, and the assignments of its Raman and infra-red active modes. The conclusions and perspective of future works are depicted in Section 4.

2. Computer methodology

First principles calculations for γ-$Cd(OH)_2$ were performed using CASTEP code [22] within the density functional theory (DFT) formalism [23,24]. The chosen LDA exchange-correlation functional was the standard parametrization of Perdew and Cerpeley [25,26]. For the GGA exchange-correlation functional we opted for the Perdew–Burke–Ernzerhof (PBE) formula [27]. The internal atomic coordinates and unit cell lattice parameters were optimized to the total minimum energy using the ultrasoft Vanderbilt-type pseudopotentials [28]. The plane-wave basis set cutoff energy for our calculations was 500 eV. The electronic valence configurations for each atomic species were: Cd-$4d^{10}5s^2$, O-$2s^22p^4$ and H-$1s^1$. Ultrasoft pseudopotentials help to reduce the computational cost of first principles electronic structure calculations by decreasing the energy cutoff of the plane-wave basis set. Results for bulk materials obtained with the PBE functional are, in general, very similar to the commonly used PW91 functional [29]. A Monkhorst–Pack [30] $4 \times 4 \times 3$ sampling was used to evaluate integrals in the reciprocal space. This Monkhorst–Pack grid is more than enough to give a well converged electronic structure due to the flatness of the γ-$Cd(OH)_2$ valence bands. In order to secure the accuracy of our results, we performed geometry optimizations using a cutoff energy of 600 eV. The comparison of both outputs revealed that an increase of 100 eV in the quality of basis set decreases the unit cell total energy by only 0.003% at most.

The structure of $Cd(H_2O)$ is shown in Fig. 1. The unit cell is monoclinic and contains four molecules. Its space group is I1m1 crystalline structure, and is arranged according to the atomic positions provided by De Wolf [1] (see Table 1). The lattice parameters position were optimized by seeking a total energy minimum for the γ-$Cd(OH)_2$ unit cell (see Table 2). The unit cell dimensions and internal atomic coordinates of γ-$Cd(OH)_2$, measured by X-ray diffraction [7], were used as input.

In order to perform the geometry optimization, the following convergence thresholds were considered for two successive self-consistent steps: total energy change smaller than 0.5×10^{-5} eV/atom, maximum force over each atom below 0.01 eV/Å, pressure smaller than 0.02 GPa, and maximum atomic displacement not exceeding 0.5×10^{-3} Å. The BFGS minimizer [31] was employed to carry out the unit cell optimization. In the BFGS scheme, a starting Hessian is recursively updated. For each self-consistent field step, the electronic minimization parameters were the following: total energy/atom convergence tolerance of 0.5×10^{-6} eV, eigen-energy threshold of 0.1923×10^{-6} eV at most, and a convergence window of 3 cycles. The plane-wave basis set cutoff energy for the calculations was chosen to be 500 eV after convergence studies, and its quality was kept fixed taking into account changes in the unit cell volume during the computer runs.

After obtaining the unit cell and atomic positions, the electronic band structure and the density of states (total and partial, and the relative contribution of each atom) were obtained for both the optimized LDA-CAPZ and GGA-PBE unit cells. Besides, the complex dielectric function $\epsilon(\omega)$ and the optical absorption $\alpha(\omega)$ of γ-$Cd(OH)_2$, for the incident light polarized on a polycrystalline sample, were calculated using the same exchange-correlation functionals of energy minimization, although replacing the ultrasoft pseudopotentials by norm-conserved ones [32–36] with an energy cutoff of 900 eV. Such replacement is necessary due to the limitations of

Table 1
Atomic parameters for the γ-$Cd(OH)_2$ crystal.

Atoms	x	y	z
Cd	0	0.1525	0
O_1	0.166(2)	0	0.489(3)
O_2	0.689(2)	0	0.942(1)
O_3	0.883(1)	0.279(6)	0.495(2)
H_1	0	0.5	0.332
H_2	0.666	0	0.25
H_3	0	0.332	0.5

Table 2
Lattice parameters for γ-$Cd(OH)_2$ crystal.

	a	b	c	α	β	γ	V
GGA	5.721	10.212	3.443	90.000	88.300	90	201.032
LDA	5.561	9.846	3.305	90.000	84.740	90	180.212
EXP	5.664	10.223	3.404	90.000	91.520	90	197.057

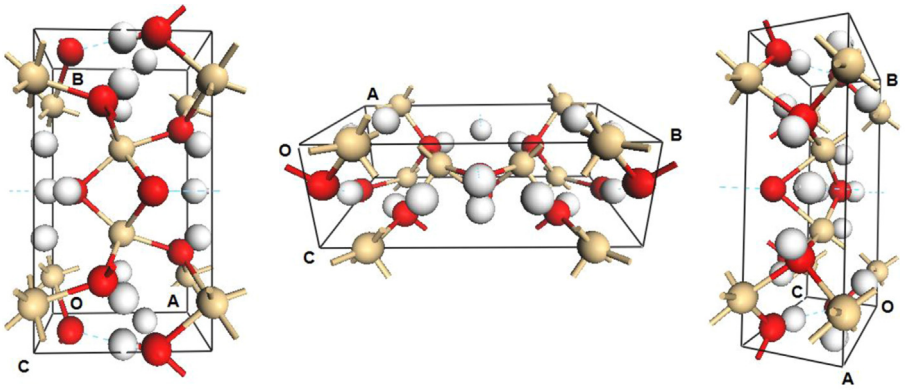

Fig. 1. The γ-$Cd(OH)_2$ crystal monoclinic unit cell.

the CASTEP code to include non-local correlation energy contributions to the optical properties using ultrasoft pseudopotentials.

3. Results and discussions

The lattice parameters of γ-$Cd(OH)_2$, calculated after geometry optimization through the DFT-LDA and DFT-GGA approaches, are shown in Table 2, together with the experimental data of Riou et al [7]. In both cases, a good agreement with the experimental data is observed. The lattice parameters calculated within the GGA approach are consistently bigger compared to those calculated using the LDA one and the experimental data, which is coherent with the results found for other compounds and the well known underbinding effect for this kind of functional.

After geometry convergence using the LDA-CAPZ (GGA-PBE) functional, the computed average pressure on the unit cell was -0.0038 GPa (-0.0137 GPa), and the hydrostatic symmetrized stress tensor components were: $\epsilon_{xx}=-0.001249$ GPa (0.019180 GPa), $\epsilon_{yy}=$ 0.009956 GPa (0.019984 GPa), $\epsilon_{zz}=0.002700$ GPa (0.002041 GPa), $\epsilon_{xz}=0.005893$ GPa (-0.011766 GPa). It is a very well-known fact that the LDA-CAPZ (GGA-PBE) exchange-correlation functional tends to overestimate (underestimate) the interatomic forces, thus predicting smaller (larger) bond lengths and lattice parameters in general.

Curves depicting the Kohn–Sham electronic band structures and partial density of states per orbital of orthorhombic γ-$Cd(OH)_2$ using the LDA-CAPZ and GGA-PBE exchange-correlation functionals are shown in Figs. 2 and 3. The Fermi level energy, corresponding to zero eV, was chosen to coincide with the maximum valence band energy. In Fig. 2, one can see the LDA-CAPZ band structure for the energy range including all calculated valence states and twelve conduction bands, with a direct band gap of 1.53 eV. Deep valence levels appear in the energy range between -18.9 eV and -17.1 eV, formed mainly from s and p orbitals (the latter contribution being much smaller than the first one). There is a large gap of about 9.4 eV. Besides, one can find the energy range -7.7 eV and 0 eV, formed from s, p and d orbitals. Observe that the contribution of the orbital p is greater than the contribution of the orbital s, while the contribution of the orbital d is greater than the contribution of the orbital p between the energy range -7.7 eV and -5.3 eV. The bottom of the conduction band has a parabolic minimum at the Γ point in the reciprocal space. Band curves between 1.53 and 5.3 eV are formed by s and p states, with similar contributions. However, above 5.3 eV, the s states become dominant in the energy range between 5.3 eV and 7.3 eV. From this point the trend is reversed, since the p state contributions become dominant to determine the character of the conduction band curves therein.

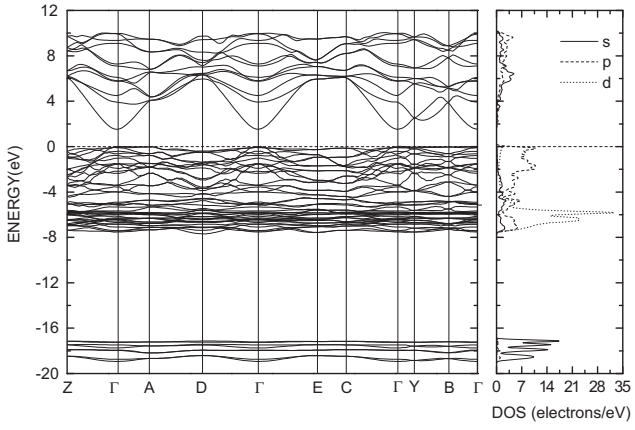

Fig. 2. γ-$Cd(OH)_2$ Kohn–Sham band structure and partial density of states (PDOS) for the full energy range using the LDA-CAPZ exchange-correlation functional.

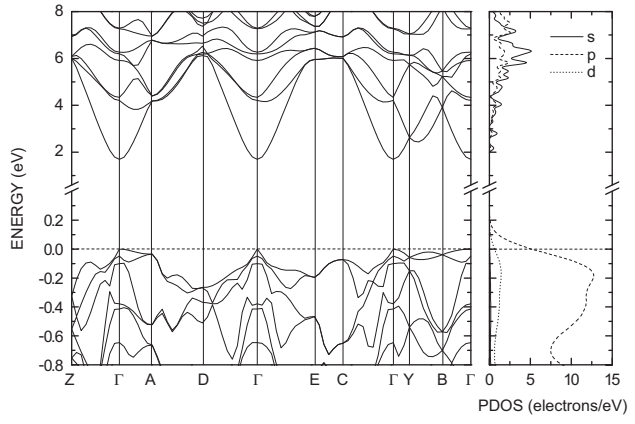

Fig. 3. Electronic band structure for γ-$Cd(OH)_2$ and partial density of states (PDOS) near the Fermi level (chosen to be zero) calculated within the GGA-PBE approach.

Fig. 3 shows the GGA-PBE Kohn–Sham band structures near the main band gap. According to our results for GGA-PBE exchange-correlation functional, γ-$Cd(OH)_2$ has a direct band gap of 1.7 eV. The smaller conduction bands for LDA-CAPZ calculations are about 0.17 eV below the GGA-PBE corresponding bands. The valence band maximum is at the Γ point in the reciprocal space, with a secondary maximum between Y and B points. On the other hand, the conduction band minimum is at the Γ point, with secondary minima located approximately at the Y point. Due to the approximations assumed in the construction of the DFT functionals, the calculated band gaps are very rough and in general much smaller than the experimental data. Indeed, the electronic eigen-energies from the DFT's Kohn–Sham calculations do not match the correct excitation energies, and a correct band gap prediction can be made only by using the exact (and unknown) expression for the non-analytic exchange-correlation functional, as it was pointed out by Perdew and Levy [37].

Fig. 4 depicts the electronic partial density of states (PDOS) for the Cd, O and H atomic species, after the calculations within the GGA exchange-correlation functional. The most relevant contribution from the Cd atoms to the electronic structure of γ-$Cd(OH)_2$ is a d DOS band that correspond to deep levels with maxima at -5.8 eV (42.3 eV^{-1}) between -7.04 and -5.41 eV, and a s DOS band at 9.6 eV (5.3 eV^{-1}) between 9.3 and 10.3 eV. The Sn DOS bands have maxima always smaller than 0.60 eV^{-1}, with three main p DOS bands: the first one between -18.0 and -15.3 eV, the

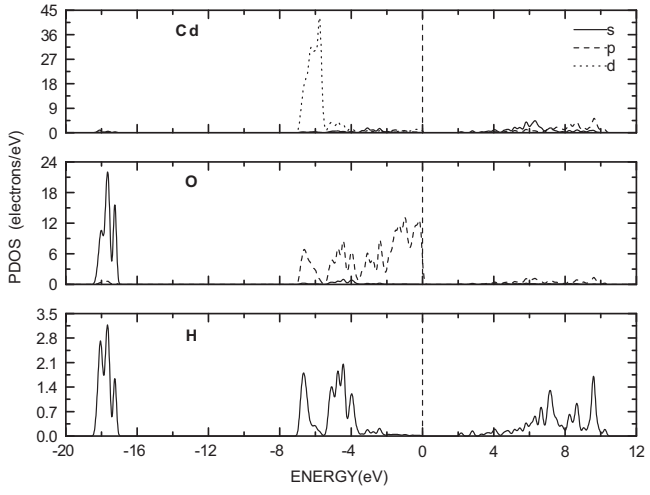

Fig. 4. Electronic partial density of states (PDOS) of γ-$Cd(OH)_2$ with per atom and per orbital contributions indicated.

second between −5.0 and 0.0 eV, and the third between 5.0 and 8.5 eV. The s DOS bands correspond to deep levels with maxima at −17.6 eV (0.37 eV^{-1}), −7.0 eV (0.4 eV^{-1}) and 5.5 eV (0.4 eV^{-1}). Finally, the electrons from the oxygen 2p levels dominate at the top of the valence band, with DOS larger than 0.5 eV^{-1} in the range −3.0 eV to 0.0 eV. In the conduction band, however, the p levels have a small contribution with bands between 5.0 and 6.2 eV, between 6.2 and 7.0 eV and between 7.0 and 8.3 eV. A deep s DOS band occurs with a maximum of 1.2 eV^{-1} at −16.3 eV.

The monoclinic $Cd(OH)_2$ structure optimized through the GGA-PBE approximation was used to perform density functional perturbation theory (DFPT) calculations, or linear response formalism [38] in order to obtain its vibrational properties. The geometry optimization criteria were more stringent than the one used for LDA-CAPZ calculations. For LDA calculations, within the ultrasoft pseudopotential scheme, the pseudo-wavefunctions are allowed to be as soft as possible in the core region, so that the cutoff energy can be reduced dramatically. On the other hand, the GGA calculations within the norm-conserving potential scheme, generate much softer pseudopotentials. Besides, the ultrasoft formalism is more complex and becomes almost intractable for such complex concepts as linear response implementation for phonons or NMR properties, for example. As a result, there is a number of tasks and properties that CASTEP code can address only with norm-conserving pseudopotentials, including the above-mentioned vibrational properties. Of course the relaxed structure is the same for calculations, no matter the use of either the ultrasoft or the norm-conserving pseudopotentials. The difference is solely on the accuracy of the output result.

The convergence thresholds were the following: total energy convergence tolerance smaller than 5×10^{-6} eV/atom, maximum ionic force smaller than 1×10^{-2} eV/Å, maximum ionic displacement tolerance of 5×10^{-4} Å, and maximum stress component smaller than 2×10^{-2} GPa [38,39]. For the self-consistent field calculations, the convergence criteria took into account a total energy per atom variation smaller than 5×10^{-7} eV, and the electronic eigen-energy variation smaller than 0.1923×10^{-6} eV.

The linear response provides an analytical way to compute the second derivative of the total energy with respect to a given perturbation. Depending on the nature of this perturbation, a number of properties can be calculated, namely a perturbation in the ionic positions gives the dynamical matrix and phonons; in the magnetic field yields a NMR response; in the unit cell vectors, the elastic constants; in the electric field, the dielectric response, etc. [40,41]. The infrared absorption intensities are described in terms of a dynamical matrix (also known as a Hessian) and Born effective charges (also known as atomic polarizability tensors, ATP) [42], and can be obtained by calculating the phonons at the Γ point ($\mathbf{k}=0$). Raman spectroscopy is used to study the vibrational, rotational, and other low-frequency modes in a system. It is based on the Raman effect of inelastic scattering of monochromatic light [43]. This interaction with vibrations results in the energy of incident photons being shifted up or down. The energy shift is defined by the vibrational frequency and the proportion of the inelastically scattered light is defined by the spacial derivatives of the macroscopic polarization [44]. The infrared and Raman spectra of monoclinic $Cd(OH)_2$ are shown in Figs. 5 and 6, respectively, without the presence of water molecules. Table 3 presents the predicted normal modes with the respective irreducible representations and the assignment of IR and Raman active modes.

Monoclinic $Cd(OH)_2$ has 57 normal modes at $\mathbf{k}=0$, with 27 infrared active modes, $\Gamma_{IR}=15A'+12A''$. According to Ref. [3], IR spectrum of monoclinic $Cd(OH)_2$ is characterized by 3 absorption bands at 3580, 3530 and 3240 cm^{-1} with the presence of water molecules. Schmidt and Lutz [45], on the other hand, proved by using IR and Raman spectroscopic that monoclinic $Cd(OH)_2$ has

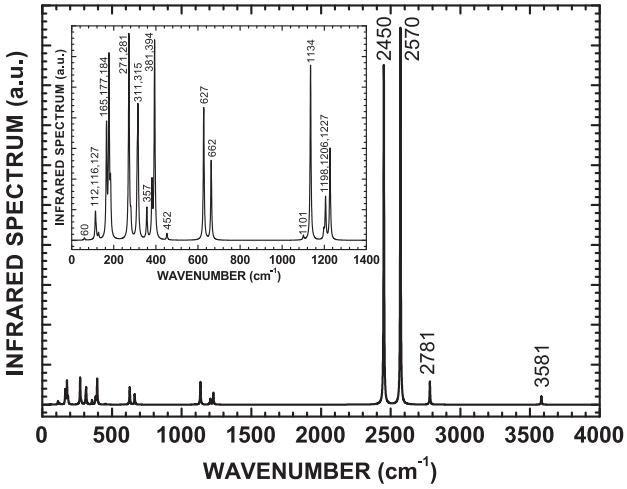

Fig. 5. Infrared spectra of monoclinic $Cd(OH)_2$ in the full range 0–4000 cm^{-1} range. The inset shows the infrared spectra in the low-frequency range 0–1400 cm^{-1} range. The numbers correspond to the normal modes shown in Table 3.

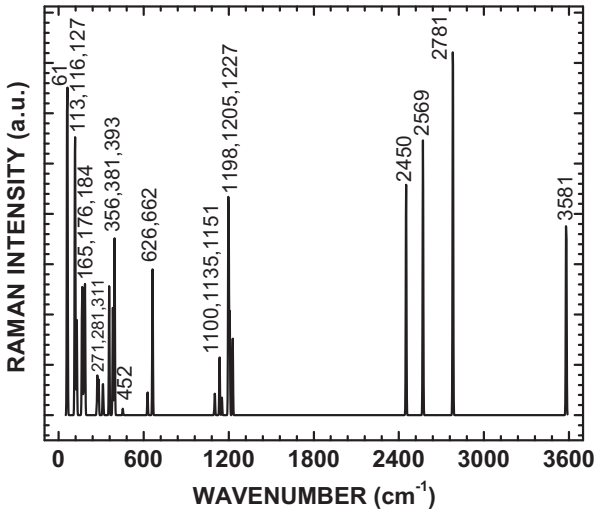

Fig. 6. Raman spectra of monoclinic $Cd(OH)_2$ in the 0–3600 cm^{-1} range. The numbers correspond to the normal modes shown in Table 3.

been characterized to be a common hydroxide and not an aquoxy-hydroxide with three crystallographically different OH^- ions. However, there is a nice agreement between both the theoretical and experimental [44] curves, mainly in the ranges of 127–200, 230–452, 900–1200 and 3500–3600 cm^{-1}, with the stretching vibration of the O–H bond being located below 455 cm^{-1} [44].

Looking at the inset of Fig. 5, depicting the low-frequency IR region, the most intense IR absorption peaks occur at 271.8 cm^{-1} (labeled as number 271 in the inset), a mode with irreducible representation (Irrep) A' which is assigned to a Cd–O–Cd bending movement along the *c*-axis and a O–Cd–O scissors movement along the *a*-axis, within the *ab* plane. The second most intense peak appears at 393.9 cm^{-1} being assigned to a O–Cd–O bending movement in the *ab* plane and a symmetrical O–H stretching with Irrep A'. The third most intense occurs at 177 cm^{-1}, corresponding to a O–Cd–O bending movement along the *b*-axis, within the *ac* plane. In the high-frequency region, the most intense IR absorption peaks occur at 2570.2 cm^{-1}, a mode with Irrep A'' which is assigned to a stretching of the OH bond. At 2450.8 cm^{-1}, an intense absorption peak is also noted, being assigned to a stretching of the OH bond along the *a*-axis.

Fig. 6 presents the calculated Raman scattering spectrum. There are 27 Raman active modes at $\mathbf{k}=0$ with $\Gamma_{Raman}=15A'+12A''$. In the

Table 3
Normal modes of monoclinic $Cd(OH)_2$ at $\mathbf{k}=0$. Irreducible representations (Irrep) are indicated, as well as the IR and Raman active modes.

N	k (cm^{-1})	Irrep	IR	Raman
1	31.0	A″	N	N
2	46.6	A′	N	N
3	48.8	A″	N	N
4	60.4	A″	Y	Y
5	71.4	A″	N	N
6	103.3	A′	N	N
7	113.3	A′	Y	Y
8	116.4	A″	Y	Y
9	116.4	A′	N	N
10	127.5	A′	Y	Y
11	129.5	A′	N	N
12	149.4	A′	N	N
13	165.6	A′	Y	Y
14	176.1	A″	Y	Y
15	179.1	A″	N	N
16	184.7	A′	Y	Y
17	203.4	A′	N	N
18	262.7	A″	N	N
19	271.9	A′	Y	Y
20	281.0	A″	Y	Y
21	299.1	A′	N	N
22	311.1	A′	Y	Y
23	314.8	A″	Y	Y
24	331.9	A″	N	N
25	348.0	A′	N	N
26	356.9	A′	Y	Y
27	366.3	A′	N	N
28	381.5	A″	Y	Y
29	382.9	A″	N	N
30	393.9	A′	Y	Y
31	402.3	A″	N	N
32	452.6	A″	Y	Y
33	463.6	A′	N	N
34	626.9	A″	Y	Y
35	649.5	A″	N	N
36	662.8	A′	Y	Y
37	663.3	A′	N	N
38	1100.8	A″	Y	Y
39	1111.0	A″	N	N
40	1135.0	A′	Y	Y
41	1136.7	A′	N	N
42	1151.6	A″	Y	Y
43	1157.8	A″	N	N
44	1185.5	A′	N	N
45	1198.1	A′	Y	Y
46	1204.8	A″	N	N
47	1205.8	A″	Y	Y
48	1221.5	A′	N	N
49	1227.3	A′	Y	Y
50	2450.7	A′	Y	Y
51	2475.9	A′	N	N
52	2569.9	A″	Y	Y
53	2640.7	A″	N	N
54	2781.2	A′	Y	Y
55	2802.3	A′	N	N
56	3581.3	A′	Y	Y
57	3581.4	A′	N	N

low-frequency region, the most intense Raman absorption peaks occur at 60.4 (labeled as number 61), being assigned to the out-of-plane bending of O–Cd–O along the *c*-axis with Irrep A''. The second most intense peak appears at 116.4 (labeled as number 116) is related again to the out-of-plane bending of O–Cd–O with Irrep A''. In the high-frequency region, the most intense Raman absorption peaks occur at 2781.3 cm^{-1} (number 2781), a mode with Irrep A' which is assigned to a stretching of the OH bond, as shown in Ref. [45]. The second most intense peak appears at 2569.9 cm^{-1} (numbers 2569) related again with a stretching of the OH bond which corresponds to a A'' mode, as shown in Ref. [45].

Finally, there are 17A' and 13A'' vibrational modes not detectable by infrared or Raman measurements. The optical permittivity tensor components calculated for monoclinic $Cd(OH)_2$ at $\omega=0$ ($\omega=\infty$) are the following: $\epsilon_{xx}=8.29791$ (3.19679), $\epsilon_{yy}=11.01577$ (3.68842), $\epsilon_{zz}=8.81789$ (3.35905), $\epsilon_{xz}=\epsilon_{zx}=-1.63707$ (-0.06105), and $\epsilon_{xy}=\epsilon_{yz}=0$ (0). On the other hand, the tensor of polarizabilities (in $Å^3$) for the static $\omega=0$, (optical $\omega=\infty$) has components: $p_{xx}=$ 122.83108 (36.97423), $p_{yy}=168.57548$ (45.24876), $p_{zz}=131.58296$ (39.70512), $p_{xz}=p_{zx}=-27.55360$ (1.02761), and $p_{xy}=p_{yz}=0$ (0).

4. Conclusions

In this work, we have obtained the structural, electronic, optical and vibracional properties of γ-$Cd(OH)_2$ using quantum chemical first-principles calculations. The structural parameters of γ-$Cd(OH)_2$, calculated after geometry optimization, show a good agreement with the experimental data. The GGA approximation overestimates the actual γ-$Cd(OH)_2$ lattice parameters by 1% at most, while the LDA lattice parameters are underestimated by $\sim 1.7\%$. The monoclinic γ-$Cd(OH)_2$ crystal has an LDA (GGA) direct band gap of 1.53 eV (1.7 eV) involving $\Gamma \rightarrow \Gamma$ transition from valence to conduction band.

We have also obtained the infrared and Raman spectra, both exhibiting a very good agreement with the experimental data [45], with the most intense infrared absorption peak near 2570 cm^{-1}, and the second peak at about 2450.8 cm^{-1} being assigned to a stretching of the OH bond. The calculated Raman spectrum exhibits the most intense peak at 2781 cm^{-1} corresponding to a stretching of the OH bond related with a A' vibrational mode.

Acknowledgments

This work was partially financed by the Brazilian Research Agencies CAPES (Rede NanoBioTec) and CNPq (INCT-Nano(Bio) Simes, Casadinho/Procad and PNPD).

References

[1] P.M. De Wolf, Acta Cryst. 21 (1966) 432.
[2] O. Glemer, U. Hauschild, H. Richert, Z. Anorg. Chem. 290 (1957) 58.
[3] A. Lecerf, A. Riou, Y. Cudennce, Y. Gerault, Mater. Res. Bull. 23 (1988) 1479.
[4] Y. Cudennec, A. Lecerf, A. Riou, Y. Gerault, Mater. Res. Bull. 24 (1989) 381.
[5] Y. Cudennec, Y. Gerault, A. Lecerf, Mater. Res. Bull. 34 (1999) 1558.
[6] Z.-X. Yang, W. Zhong, Y.-X. Yin, X. Du, Y. Deng, C. Au, Y.-W. Du, Nanoscale Res. Lett. 42 (2010) 961.
[7] A. Riou, Y. Cudennec, Y. Gerault, Mater. Res. Bull. 25 (1990) 987.
[8] M. Ristic, S. Poporic, S. Music, Mater. Lett. 58 (2004) 2494.
[9] H. Zhang, X.Y. Ma, Y.J. Ji, J. Xu, D.R. Yang, Mater. Lett. 59 (2005) 56.
[10] S. Motupally, M. Jain, V. Srinivasan, J.W. Weidner, J. Electrochem. Soc. 145 (1998) 34.
[11] B. Tang, L.H. Zhuo, J.C. Ge, J.Y. Niu, Z.Q. Shi, Inorg. Chem. 44 (2005) 2568.
[12] H.Z. Zhong, Y.C. Li, Y. Zhou, C.H. Yang, Y.F. Li, Nanotechnology 17 (2006) 772.
[13] Y.Z. Zhang, G.L. Wang, Mater. Lett. 62 (2008) 673.
[14] R. Ferro, I.A. Rodriguez, Sol. Energy Mater. Sol. Cells 64 (2000) 363.
[15] T.K. Subramanyam, S. Uthanna, N.B. Srinivasulu, Mater. Lett. 35 (1998) 214.
[16] A.K. Srivastava, S. Pandey, K.N. Sood, S.K. Halder, R. Kishore, Mater. Lett. 62 (2008) 727.
[17] F. Zhang, L. Bei, J.M. Cao, X. Wang, J. Solid State Chem. 181 (2008) 143.
[18] T. Ghoshal, S. Biswas, P.M.G. Nambissan, G. Majumdar, S.K. De, Cryst. Growth Des. 9 (2009) 1287.
[19] Z.Y. Jia, Y.W. Tang, L.J. Luo, B.H. Li, Cryst. Growth Des. 8 (2008) 2116.
[20] X.L. Liu, C. Li, S. Han, J. Han, C.W. Zhou, Appl. Phys. Lett. 82 (2003) 12.
[21] M.F. Ye, H.Z. Zhong, W.J. Zheng, R. Li, Y.F. Li, Langmuir 23 (2007) 90649.
[22] M.D. Segall, P.L.D. Lindan, M.J. Probert, C.J. Pickard, P.J. Hasnip, S.J. Clark, M.C. Payne, J. Phys.: Condens. Matter 14 (2002) 2717.
[23] P. Hohenberg, W. Kohn, Phys. Rev. 136 (1964) B864.
[24] W. Kohn, L.J. Sham, Phys. Rev. 140 (1965) A1133.
[25] J.P. Perdew, A. Zunger, Phys. Rev. B 23 (1981) 5048.
[26] D.M. Ceperley, B.J. Alder, Phys. Rev. Lett. 45 (1980) 566.
[27] J.P. Perdew, K. Burke, M. Ernzerhof, Phys. Rev. Lett. 77 (1996) 3865.
[28] D. Vanderbilt, Phys. Rev. B 41 (1990) 7892.

[29] J.P. Perdew, J.A. Chevary, S.H. Vosko, K.A. Jackson, M.R. Pederson, D.J. Singh, C. Fiolhais, Phys. Rev. B 46 (1992) 6671.
[30] H.J. Monkhorst, J.D. Pack, Phys. Rev. B 13 (1976) 5188.
[31] B.G. Pfrommer, M. Cote, S.G. Louie, M.L. Cohen, J. Comput. Phys. 131 (1997) 133.
[32] J.S. Lin, A. Qteish, M.C. Payne, V. Heine, Phys. Rev. B 47 (1993) 4174.
[33] J.M. Henriques, E.W.S. Caetano, V.N. Freire, J.A.P. da Costa, E.L. Albuquerque, Chem. Phys. Lett. 427 (2006) 113.
[34] J.M. Henriques, E.W.S. Caetano, V.N. Freire, J.A.P. da Costa, E.L. Albuquerque, J. Solid State Chem. 180 (2007) 974.
[35] J.M. Henriques, E.W.S. Caetano, V.N. Freire, J.A.P. da Costa, E.L. Albuquerque, J. Phys.: Condens. Matter 19 (2007) 106214.
[36] C.A. Barboza, J.M. Henriques, E.L. Albuquerque, E.W.S. Caetano, V.N. Freire, J. Phys. D: Appl. Phys. 42 (2009) 155406.
[37] J.P. Perdew, M. Levy, Phys. Rev. Lett. 51 (1983) 1884.
[38] E. Moreira, J.M. Henriques, D.L. Azevedo, E.W.S. Caetano, V.N. Freire, E.L. Albuquerque, J. Solid State Chem. 184 (2011) 921.
[39] E. Moreira, J.M. Henriques, D.L. Azevedo, E.W.S. Caetano, V.N. Freire, U.L. Fulco, E.L. Albuquerque, J. Appl. Phys. 112 (2012) 043703.
[40] E.L. Albuquerque, M.G. Cottam, Solid State Commun. 81 (1992) 383.
[41] C.G. Bezerra, E.L. Albuquerque, Physica A 255 (1998) 285.
[42] S. Baroni, S. de Gironcoli, A. dal Corso, P. Giannozzi, Rev. Mod. Phys. 73 (2001) 515.
[43] M. Babiker, D.R. Tilley, E.L. Albuquerque, J. Phys. C: Solid State Phys. 18 (1985) 1285.
[44] D. Porezag, M.R. Pederson, Phys. Rev. B 54 (1996) 7830.
[45] M. Schmidt, H.D. Lutz, Mater. Res. Bull. 26 (1991) 605.